Surface & Coatings Technology 350 (2018) 954–961

Contents lists available at ScienceDirect

Surface & Coatings Technology

journal homepage: www.elsevier.com/locate/surfcoat

Study of W-Co ODS coating on stainless steels by mechanical alloying

Chun-Liang Chen*, Sutrisna

Department of Materials Science and Engineering, National Dong Hwa University, Hualien 97401, Taiwan

ARTICLE INFO

Keywords:
WC-Co coating
Mechanical alloying
Dispersion strengthening
Wear resistance

ABSTRACT

Tungsten-based coatings have attracted considerable interest in recent years for industrial applications because of superior wear resistance. In this study, the W-Co oxide dispersion strengthened (ODS) coating on stainless steels by mechanical alloying (MA) has been investigated. The different reinforced particles (Y_2O_3, TiC) have been introduced to the W-Co coating layer as dispersion strengthening during mechanical alloying. The results showed that the formation of the (W,Co)C, Co_7W_6 and Co_3W phases was generated after a long milling duration. The use of Y_2O_3 dispersed particles in the coating layer demonstrated homogenous distribution of microstructure and an increase of mechanical properties. However, the coating with TiC reinforcement has a significant change in distribution of the microstructure and composition and formed voids or micro-cracks, which decrease densification and hardness of the coating materials. The W-Co ODS coating by mechanical alloying is one of the most promising coating methods for enhanced wear resistance on stainless steels.

1. Introduction

Tungsten alloys have attractive property combinations of high strength at elevated temperature, superior wear resistance, low thermal expansion, high thermal conductivity and low sputtering yield [1–3]. Therefore, they are ideal materials for many industrial applications such as cutting and drilling tools, wear resistant components, and nuclear fusion reactors [2,4–6]. The presence of Co in W alloys can act as a binder to provide excellent wetting properties at sintering temperature, and thus aids full densification and refines the microstructure of materials [7,8]. In addition, Co is soluble in W and enhances mechanical properties via solid-solution strengthening [9]. However, tungsten alloys have some major drawbacks including their inherently high ductile-brittle transition temperature (DBTT) and low recrystallization temperature [10]. In recent years, the addition of oxides or carbides uniformly dispersed in the tungsten matrix fabricated by mechanical alloying has been widely studied [9–13]. The oxide dispersoids play an important role in improving ductile-brittle transition temperature (DBTT), recrystallization temperature, wear resistance, creep strength and irradiation resistance of tungsten alloys [14]. In this study, the W-Co coating reinforced with Y_2O_3 and TiC particles on stainless steel balls produced by mechanical alloying was investigated. It has been reported that coatings by mechanical alloying method can promote supersaturated solid solution, nanostructured grain, formation of intermetallics and in-situ oxide dispersoids [15,16]. Therefore, the aim of this study is to investigate synthesis and characteristics of the W–Co-Y_2O_3 and W-Co-TiC coatings on stainless steel balls by mechanical alloying. In addition, formation of in-situ WC by the interaction of tungsten matrix and carbon contamination during ball milling has been also investigated in this study.

2. Experimental procedure

Tungsten and cobalt (99.9% purity, size 15–50 μm) elemental powders are used as matrix of a coating material reinforced with yttrium oxide (Y_2O_3) powders (99.99% purity, size: 20–50 nm), and titanium carbide (TiC) powders (99.50% purity size: 40–50 μm). The W-Co coating materials with the different reinforcements were designed and have the composition of W-12Co-2Y_2O_3 and W-12Co-2TiC (in weight percent). The W-Co materials have been coated on the SUS 304 ball in 8 mm as a substrate. The coating layers were produced by the mechanical alloying technique (Retsch PM100 instrument) with the ball to powder ratio (BRP) of 10: 1 and 350 rpm of speed under an argon atmosphere for different durations; 4 h, 8 h, 16 and 24 h. The vial material used in this study was tungsten carbide. The phase constitutions of powders at the different milling times were determined by using X'Pert Pro X-ray diffraction (XRD). Scanning electron microscope (Hitachi-4700) with energy dispersive spectroscopy (EDS) was used to examine microstructure evolution and chemical composition of the different coating layers. Vickers hardness measurements were performed at room temperature using a load of 1 kg for 15 s. Nanoindentation tests (MTS Nanoindenter XP) were conducted to obtain the elastic modulus and hardness using the continuous stiffness measurement (CSM) method.

* Corresponding author at: No. 1, Sec. 2, Da Hsueh Rd., Shoufeng, Hualien 97401, Taiwan.
E-mail address: chunliang@gms.ndhu.edu.tw (C.-L. Chen).

https://doi.org/10.1016/j.surfcoat.2018.03.047
Received 7 December 2017; Received in revised form 6 February 2018; Accepted 14 March 2018
Available online 17 March 2018

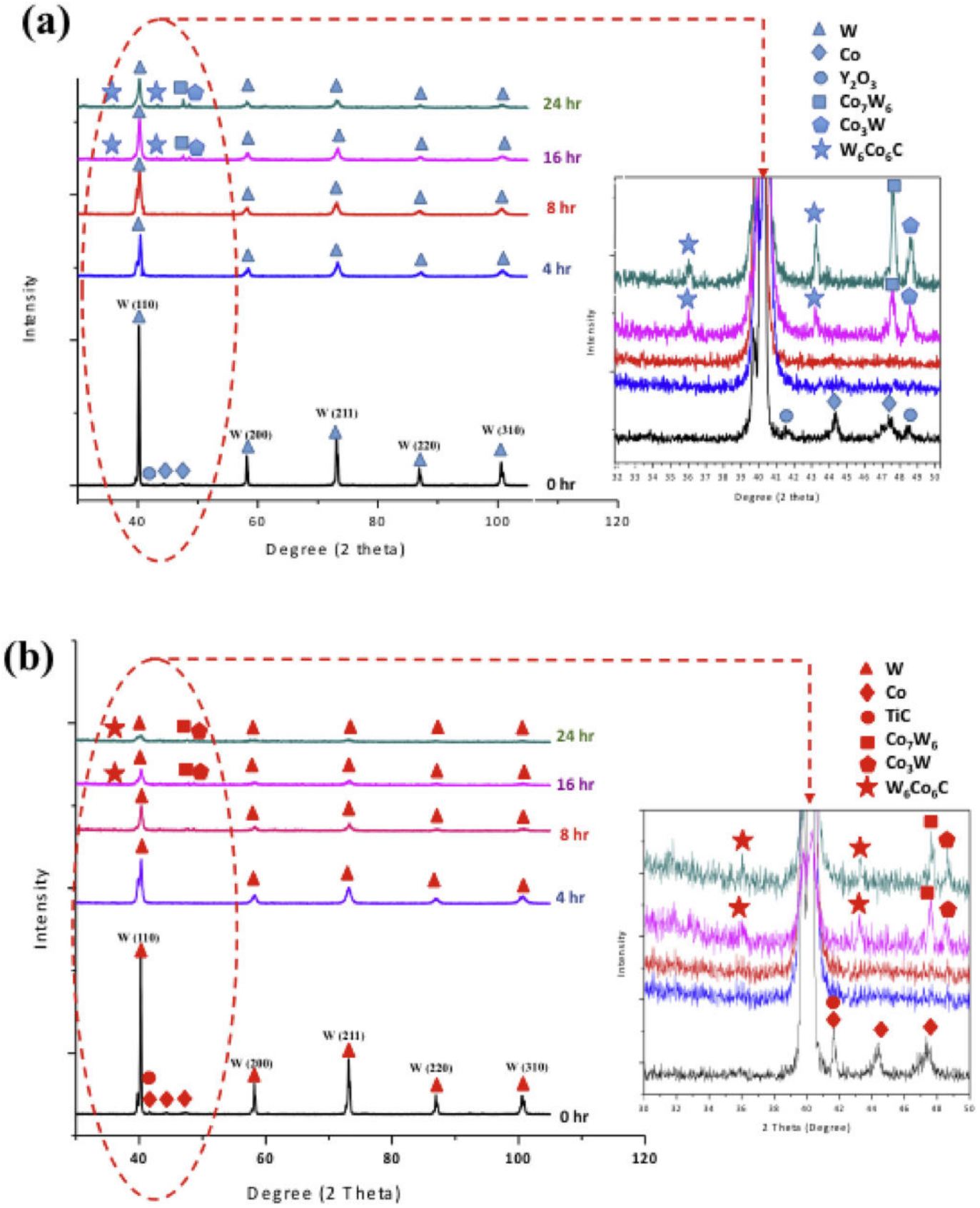

Fig. 1. XRD spectra of the (a) W-Co-Y_2O_3 and (b) W-Co-TiC powders for different milling duration; 0 h, 4 h, 8 h, 16 h and 24 h.

3. Results and discussion

3.1. Powder characterization

Fig. 1a shows the XRD spectra of the W-Co-Y_2O_3 milled powders as a function of milling time. It demonstrates that the five diffraction peaks of bcc phase in tungsten corresponding to (110), (200), (211), (220) and (310) reflections were clearly observed. Small peaks corresponding to Co were detected in the un-milled powders and then disappeared after 4 h of milling, indicating binary W-Co solid solution or refinement of the powders taking place through mechanical alloying. The peaks of tungsten become broadening and smooth with increasing the milling time, which indicates effects of lattice distortion and crystallite size. The shift of W peaks with increasing milling time is also found in the XRD spectra, see Fig. 1a), suggesting that the change of the lattice constant due to the solid solution formation and the influence of crystal defects such as interstitials, vacancies and dislocations. Furthermore, in the long milling times (16 h and 24 h), the small peaks corresponding to the Co_7W_6 and Co_3W intermetallic phases and the W_6Co_6C tungsten carbide were observed. In this study, the carbon contamination of the coatings can be generated by the vial material of tungsten carbide and thus promoted the formation of (W,Co)C at the W-Co coatings after a longer milling time.

Fig. 1b shows the XRD spectra of the W-Co-TiC milled powders as a function of milling time, which has a similar tendency as that of the W-Co-Y_2O_3 powder samples. Hoverer, there is a significant change in the peak broadening and reduction in intensity obtained in the W-Co-TiC powder samples. It indicates that the use of micro-size TiC could act as milling agents and favors the refining of the powder particle size and creates a large amount of strain energy during the milling process [17]. The results can be correlated to the variation of the crystallite size and the lattice strain in the milled powders as shown in Fig. 2. In the early stages of milling, 4 h and 8 h, the two different coating materials have almost the same crystallite size and the lattice strain. However, it becomes a large difference as the milling times increased to 16 h and 24 h. It is believed that the dispersed TiC particle plays an important role in influencing the crystallite size and the lattice strain of the W-Co alloyed powders during the process of mechanical alloying. It will be further discussed in the sections of the SEM/EDS and nanoindentation.

3.2. Characterization of W-Co coatings on stainless steel balls

3.2.1. SEM/EDS

Fig. 3 demonstrates the microstructure evaluation of the W-Co-Y_2O_3 coating deposited on the stainless ball substrate at the different milling durations. Three different regions can be clearly defined as the incomplete milling powders, coating layer, and substrate as shown in Fig. 3. A non-uniform microstructure with an irregular interface between the coating and substrate was obtained at the beginning of the milling process; see Fig. 3a and b. Homogeneous distribution of a thick coating layer has taken place as the milling times increased to 16 h and 24 h, see Fig. 3c and d. On the other hand, Fig. 4 shows the W-Co coating dispersed with TiC after milling for different times. It can be seen clearly that the coating layer contains a heterogeneous microstructure composed of a number of pores and microcracks. It implies that the use of micro-size TiC could deteriorate the bonding strength between tungsten matrix and reinforcing particles. Therefore, it has a significant influence on the densification and microstructure homogeneity of the coating.

EDS analysis was further performed for determining elemental distributions at the three regions of the model coatings as shown in Fig. 5. A high concentration of C, O and W elements was detected at the outer region of the coating; see position “A” of Fig. 5a, where particle aggregation was created by incomplete milling reactions. It is believed that the carbon/oxygen contamination can be generated by grinding media or process control agent during mechanical alloying [12]. In the position “B”, the central region of the coating contains 11.54 wt.% Co, which indicates a fairly complete solid solution of W–Co obtained by mechanical alloying. The interface between the coating and the substrate is sited at the position “C”. It can be seen clearly that the iron and chromium elements were found in the coating, which suggests that severe plastic deformation promotes the interfacial diffusion from the stainless steel substrate into the W-Co coating.

Fig. 5b shows the EDS analysis of the W-Co-TiC coating after 24 h of milling. The outer region of the coating, see position “A”, has a similar result as that of the W-Co-Y_2O_3 sample, indicating a high concentration of carbon and oxygen from processing. In the position “B”, a low content of Co about 9 wt.% was found in the middle area of the coating, which implies incomplete solid solution of W-Co and an inhomogeneous distribution of the coating composition. The position “C” is located at the dark area of the coating where a high level of C, Ti Co

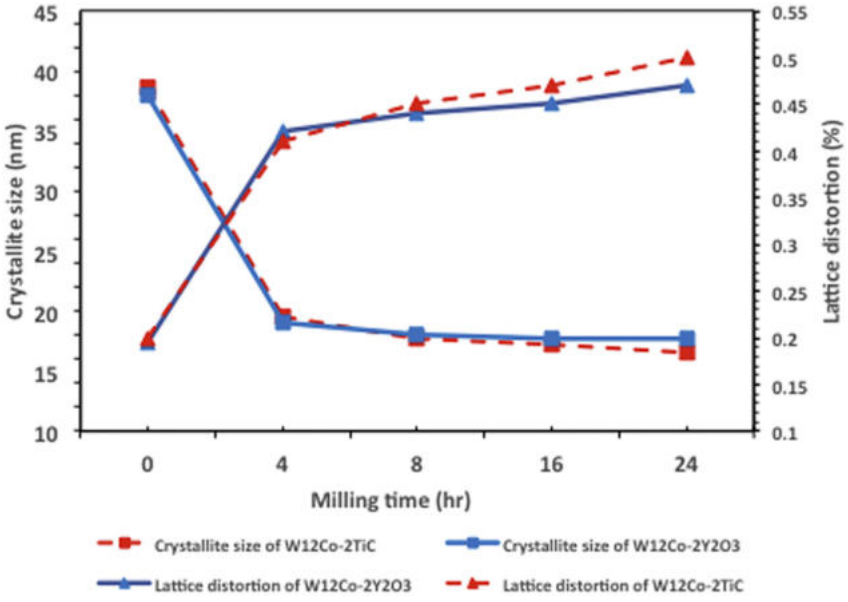

Fig. 2. Variation of crystallite size and lattice distortion of the W-Co-Y_2O_3 and W-Co-TiC powders as a function of milling time.

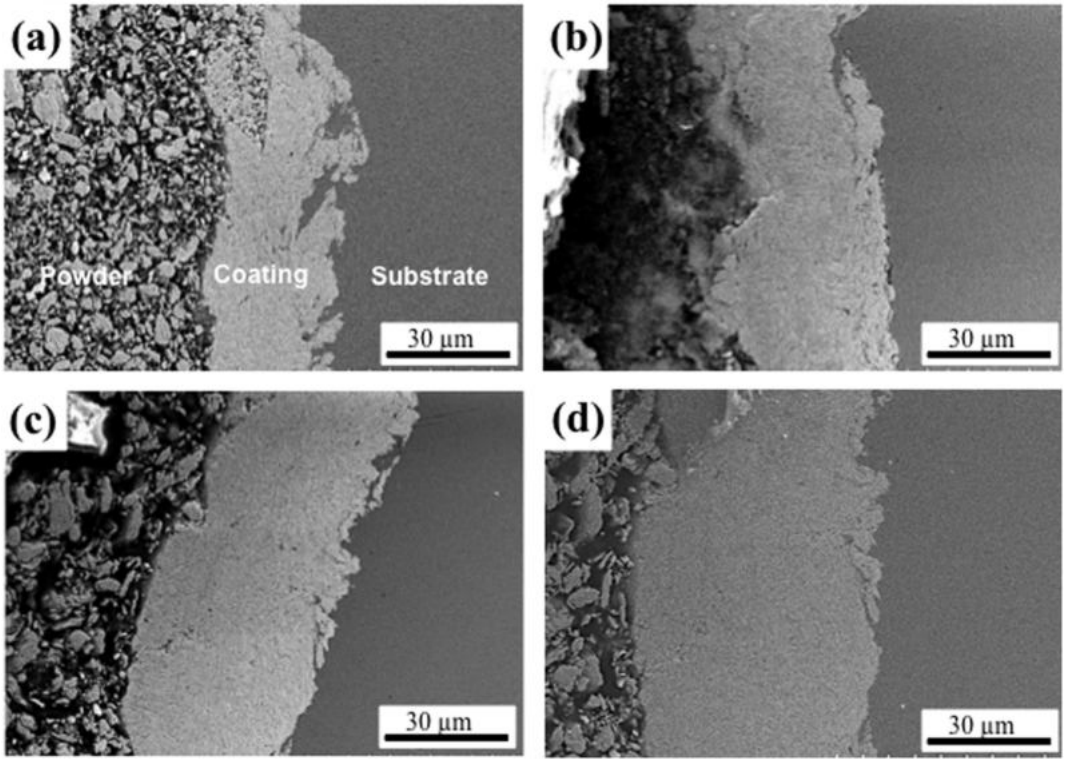

Fig. 3. SEM images of the W-Co-Y_2O_3 coating on the SUS 304 ball at (a) 4 h, (b) 8 h, (c) 16 h and (d) 24 h of milling.

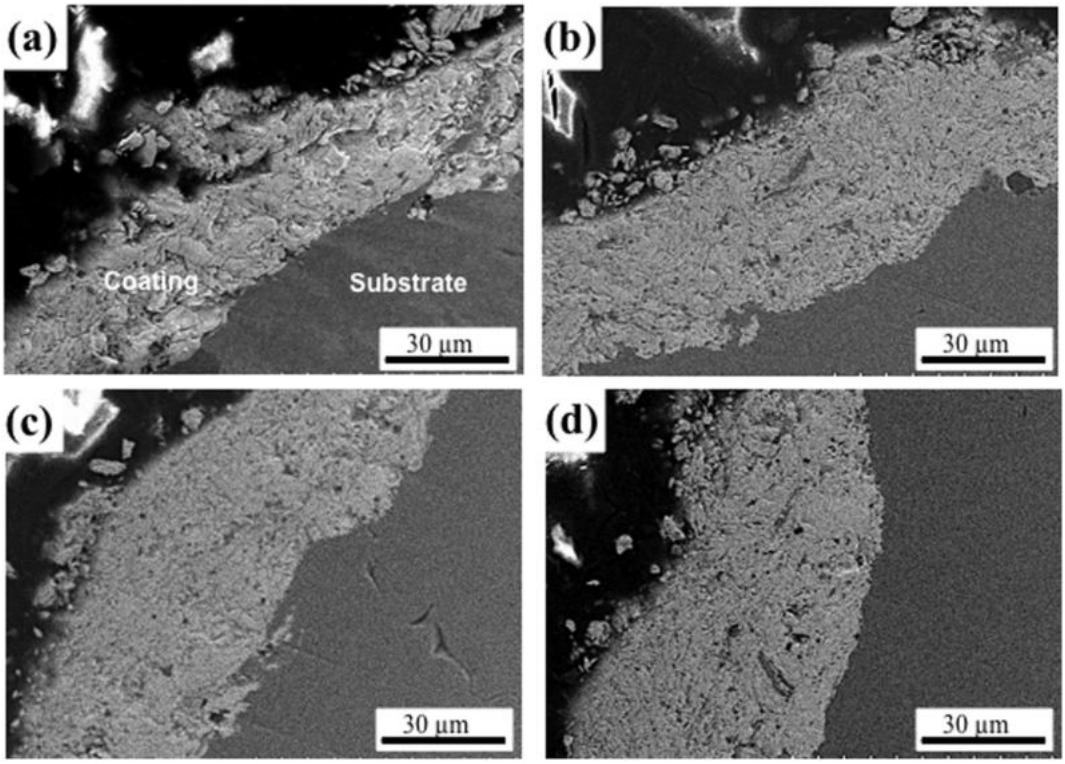

Fig. 4. SEM images of the W-Co-TiC coating on the SUS 304 ball at (a) 4 h, (b) 8 h, (c) 16 h and (d) 24 h of milling.

and W elements was obtained. It suggests that the micro-size of TiC particles can be embedded in the W and Co powders and agglomerates together to form a large particle size. Thus, the non-uniform distribution of microstructure and composition of the coating was clearly found in the case of the TiC containing samples.

3.2.2. Hardness and nanoindentation

Fig. 6 shows the distribution of Vickers hardness of the W-Co-Y_2O_3 and W-Co-TiC coatings at various cross-sectional depths. Significant increase in hardness is observed from the substrate (~450 HV) to the interface region (~850 HV). It implies that sufficiently high impact

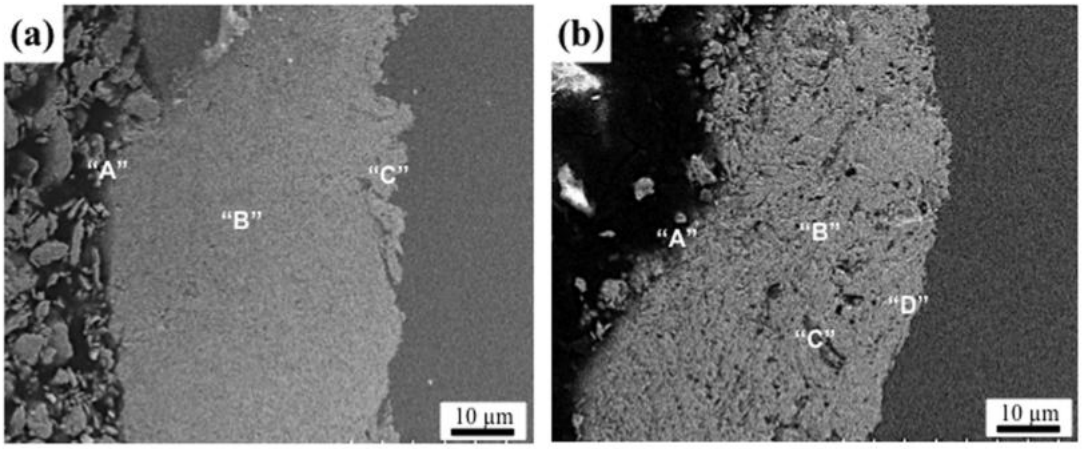

Position (wt%)	C	O	Cr	Fe	Co	W
A	46.9	9.1	-	-	-	43.8
B	-	-	-	-	11.5	88.4
C	-	-	13.4	56.0	-	30.5

Position (wt%)	C	O	Cr	Fe	Ti	Co	W
A	46.2	20.3	-	-	-	-	33.3
B	-	-	-	-	-	9.4	90.5
C	29.3	8.7	-	-	1.2	7.7	52.8
D	-	-	18.7	65.0		-	16.2

Fig. 5. EDX analysis of (a) the W-Co-Y_2O_3 and (b) W-Co-TiC powders coatings after 24 h of milling.

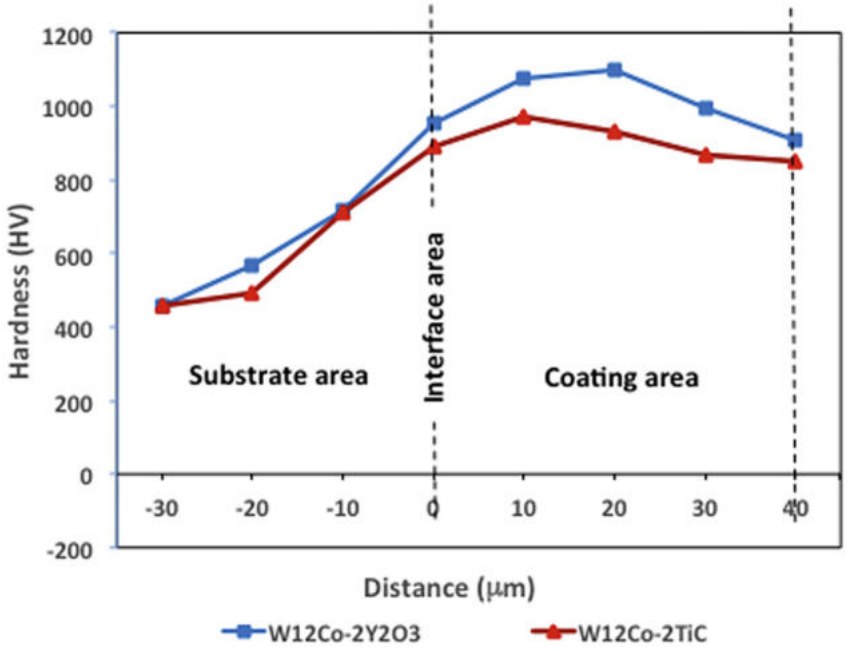

Fig. 6. The distribution of microhardness of the W-Co-Y_2O_3 and W-Co-TiC coatings at various cross-sectional depths.

energy was created at the interface during ball milling and thereby diffusivity can be accelerated between the W-Co coating and the Fe-Cr substrate. Consequently, the solid solution of iron and chromium into the W-Co coating layer can be achieved. The coating with the highest hardness about 1100 HV was found in the center region of the W-Co-Y_2O_3 sample. It can be attributed to a homogeneous distribution of microstructure with the solid solution matrix (W-Co), fine-grained structure and the formation of Co_7W_6 intermetallics and tungsten carbides in the coating by mechanical alloying. However, when the distance close to the out region of the coating, incomplete milling powders, resulting in a considerable drop of hardness (~800 HV).

Fig. 7 shows the variation of hardness of the W-Co coatings as a function of milling time. The results showed that hardness of the coatings increased as the milling time increased. After the prolonged milling times, 16 h and 24 h, a significant increase in hardness was obtained and it might correspond to grain refinement and formation of intermetallic phases as well as tungsten carbides, which has been identified by XRD spectra as shown in Fig. 1. It is believed that sufficient milling time can achieve a steady state and obtain a milled powder containing a solid solution and a homogeneous microstructure

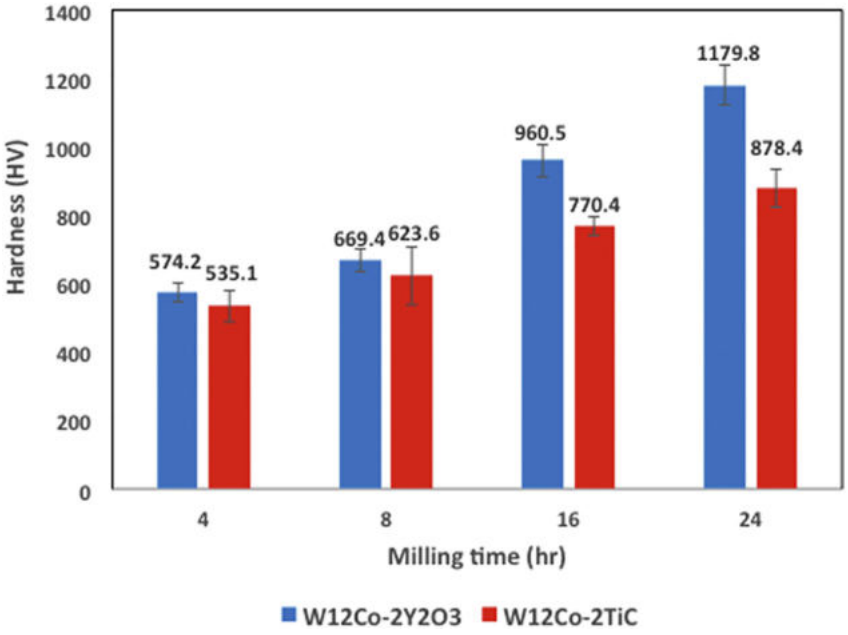

Fig. 7. The microhardness of the W-Co-Y_2O_3 and W-Co-TiC coatings at different duration of milling.

with uniformly distributed reinforcement particles. The coating with dispersed nano-Y_2O_3 oxides demonstrates the highest hardness value (1178 HV) in comparison with the TiC containing samples (878 HV). It is believed that the use of nano-Y_2O_3 oxides plays an important role in enhancing the densification and homogeneity of the coating, which can be dominated by solid-state diffusivity, chemical reactivity and the coherent interface between the W-Co matrix and nano-oxide particles during ball milling. On the other hand, although the micro-size of TiC particles can act as milling agents to effectively promote refinement of crystallite size, large lattice strain and high dislocation it also brings some problems with formation of voids and micro-crack and a heterogeneous distribution of microstructure and composition in the coating layer, leading to a dramatic decrease in hardness (535 HV–878 HV).

Nanoindentation was used to determine the hardness and elastic modulus of the W-Co coatings at different milling times and the measurements are listed in Table 1. The corresponding load-displacement curve during nanoindentation can be also seen in Fig. 8. The result shows that the W-Co-Y_2O_3 coating at 24 h of milling has the highest indentation hardness 12.07 (GPa) among the coatings. The significant increase of hardness can be contributed to high densification, uniform microstructure, and formation of the Co_7W_6 intermetallic phase and the almost complete solid solution of W–Co obtained in the Y_2O_3 containing samples. However, the W-Co-TiC coating has a much smaller hardness, which corresponds to non-uniform microstructure with voids and micro-crack and inhomogeneous composition of the coating observed in SEM investigation, see Fig. 4. In addition, the elastic modulus in nanoindentation tests is determined from a linear fit to upper portions of unloading curve. It also demonstrates that the W-Co-Y_2O_3 coating has a remarkably high elastic modulus than that of the W-Co-TiC coating. Apart from homogeneity of microstructure and composition, the interfacial bond between the reinforced particles and W-Co matrix is also important to determine elastic modulus of the coatings. In case of the present study, the large agglomerated TiC particles and formation of voids and cracks can reduce the bond strength of the reinforcement/matrix in the coating, causing a significant reduction in the elastic modulus.

Fig. 9a and b show the hardness–displacement curves of the W-Co-Y_2O_3 and W-Co-TiC coatings at different milling times. The results demonstrate that the hardness increases with increasing milling time in both coating materials, particularly at larger indentation depths (> 1000 nm). It should be noted that the indentation size effect was observed in the coating samples, which indicates that the hardness obviously decreased with the increase of indentation depth.

Table 1
Nanoindentation measurements of the W-Co-Y_2O_3 and W-Co-TiC coatings for different milling times.

No	Coating Materials (Nanoindention)	Hardness (GPa)	Elastic Modulus (GPa)
1	W12Co-2Y_2O_3 (4 h)	7.62	244.8
	W12Co-2Y_2O_3 (8 h)	7.75	287.7
	W12Co-2Y_2O_3 (16 h)	10.68	250.6
	W12Co-2Y_2O_3 (24 h)	12.07	317.4
2	W12Co-2TiC (4 h)	3.26	132.6
	W12Co-2TiC (8 h)	4.37	148.4
	W12Co-2TiC (16 h)	5.22	159.7
	W12Co-2TiC (24 h)	6.65	189.0

4. Conclusions

In this study, the W-Co-Y_2O_3 and W-Co-TiC coatings on the 304 stainless steel substrates by mechanical alloying were investigated. The XRD results show that binary W-Co solid solution takes place through mechanical alloying after 4 h of milling and the formation of Co_7W_6, and Co_3W intermetallic phases was found at the final stage of milling. The formation of the (W,Co)C tungsten carbide was caused by carbon contamination from grinding media after a long milling duration. There is a large change in the peak broadening and reduction in intensity obtained in the W-Co-TiC powder samples, suggesting TiC could act as milling agents and favors the refining of the powder particle size and creates a large amount of strain energy. The results also indicate that the coating dispersed with nano-Y_2O_3 oxides can promote a homogenous distribution of microstructure and composition, resulting in a significant increase in hardness. However, the micro-size of TiC particles can be embedded in the W and Co powders and agglomerates together to form a large particle size. A significant change in distribution of the microstructure and composition can be obtained in the coating. In addition, TiC could deteriorate the bonding strength between tungsten matrix and reinforcing particles and formed voids or micro-cracks, which decrease densification, hardness and elastic modulus of the

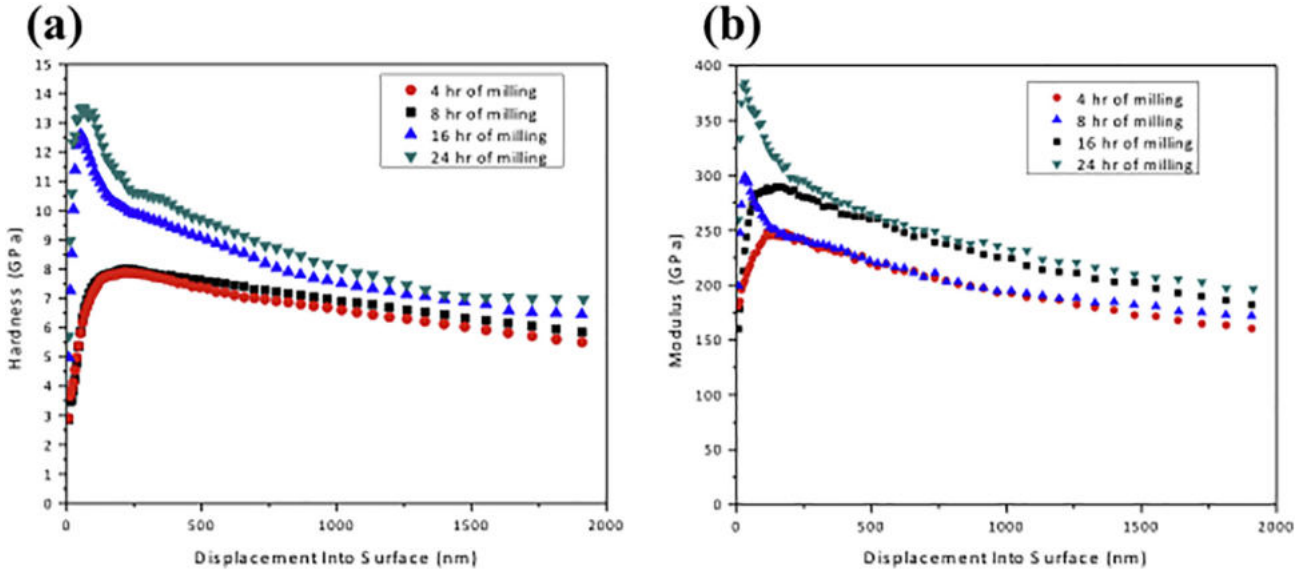

Fig. 8. A typical load-displacement curve of the W-Co-Y_2O_3 coating for different milling times of (a) 4 h, (b) 8 h, (c) 16 h, and (d) 24 h.

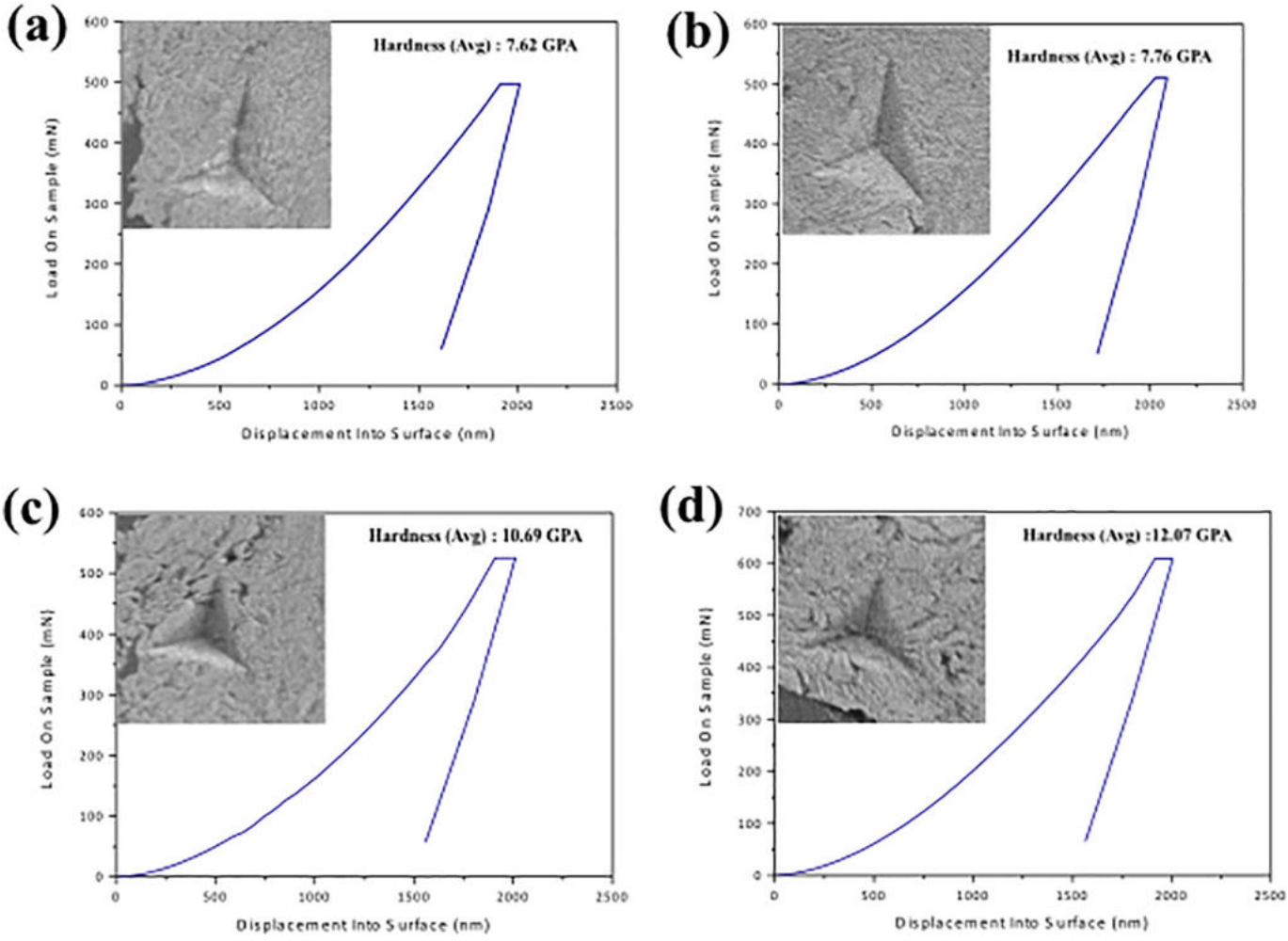

Fig. 9. The hardness–displacement curve of (a) the W-Co-Y_2O_3 and (b) W-Co-TiC coatings at different milling times.

coating materials.

Acknowledgements

The authors would like to gratefully acknowledge financial support from Ministry of Science and Technology (MOST) Taiwan under the grant MOST 106-2221-E-259-015-MY2.

References

[1] A. Krella, A. Czyzniewski, Cavitation resistance of Cr-N coatings deposited on austenitic stainless steel at various temperatures, Wear 266 (2009) 800–809, http://dx.doi.org/10.1016/j.wear.2008.11.002.

[2] P. Norajitra, L.V. Boccaccini, E. Diegele, V. Filatov, A. Gervash, R. Giniyatulin, S. Gordeev, V. Heinzel, G. Janeschitz, J. Konys, W. Krauss, R. Kruessmann, S. Malang, I. Mazul, A. Moeslang, C. Petersen, G. Reimann, M. Rieth, G. Rizzi, M. Rumyantsev, R. Ruprecht, V. Slobodtchouk, Development of a helium-cooled divertor concept: design-related requirements on materials and fabrication technology, J. Nucl. Mater. 329–333 ((2004) 1594–1598, http://dx.doi.org/10.1016/j.jnucmat.2004.04.137.

[3] C.L. Chen, Y. Zeng, Synthesis and characteristics of W-Ti alloy dispersed with Y2Ti2O7 oxides, Int. J. Refract. Met. Hard Mater. 56 (2016) 104–109, http://dx.doi.org/10.1016/j.ijrmhm.2015.12.008.

[4] S. Wurster, N. Baluc, M. Battabyal, T. Crosby, J. Du, C. García-Rosales, A. Hasegawa, A. Hoffmann, A. Kimura, H. Kurishita, R.J. Kurtz, H. Li, S. Noh, J. Reiser, J. Riesch, M. Rieth, W. Setyawan, M. Walter, J.H. You, R. Pippan, Recent progress in R&D on tungsten alloys for divertor structural and plasma facing materials, J. Nucl. Mater. 442 (2013) 181–189, http://dx.doi.org/10.1016/j.jnucmat.2013.02.074.

[5] M. Rieth, S.L. Dudarev, S.M. Gonzalez De Vicente, et al., Recent progress in research on tungsten materials for nuclear fusion applications in Europe, J. Nucl. Mater. 432 (2013) 482–500, http://dx.doi.org/10.1016/j.jnucmat.2012.08.018.

[6] C. Suryanarayana, N. Al-Aqeeli, Mechanically alloyed nanocomposites, Prog. Mater. Sci. 58 (2013) 383–502, http://dx.doi.org/10.1016/j.pmatsci.2012.10.001.

[7] J.M. Marshall, M. Giraudel, The role of tungsten in the Co binder: effects on WC grain size and hcp-fcc Co in the binder phase, Int. J. Refract. Met. Hard Mater. 49 (2015) 57–66, http://dx.doi.org/10.1016/j.ijrmhm.2014.09.028.

[8] L.M. Luo, X.Y. Tan, H.Y. Chen, G.N. Luo, X.Y. Zhu, J.G. Cheng, Y.C. Wu, Preparation and characteristics of W-1wt.% TiC alloy via a novel chemical method and spark plasma sintering, Powder Technol. 273 (2015) 8–12, http://dx.doi.org/10.1016/j.powtec.2014.12.033.

[9] H. Myalska, R. Swadźba, R. Rozmus, G. Moskal, J. Wiedermann, K. Szymański, STEM analysis of WC-Co coatings modified by nano-sized TiC and nano-sized WC addition, Surf. Coat. Technol. 318 (2017) 279–287, http://dx.doi.org/10.1016/j.surfcoat.2017.01.072.

[10] C. Suryanarayana, E. Ivanov, V.V. Boldyrev, The science and technology of mechanical alloying, Mater. Sci. Eng. A 304–306 (2001) 151–158, http://dx.doi.org/10.1016/S0921-5093(00)01465-9.

[11] C.L. Chen, Y. Zeng, Influence of Ti content on synthesis and characteristics of W-Ti ODS alloy, J. Nucl. Mater. 469 (2016) 1–8, http://dx.doi.org/10.1016/j.jnucmat.2015.11.018.

[12] C.L. Chen, C.L. Huang, The effects of alloying and milling on the formation of intermetallics in ODS tungsten heavy alloys, Intermetallics 41 (2013) 10–15, http://dx.doi.org/10.1016/j.intermet.2013.04.014.

[13] A. Canakci, F. Erdemir, T. Varol, R. Dalmiş, S. Ozkaya, Effects of a new pre-milling coating process on the formation and properties of an Fe-Al intermetallic coating, Powder Technol. 268 (2014) 110–117, http://dx.doi.org/10.1016/j.powtec.2014.08.034.

[14] I. Wesemann, W. Spielmann, P. Heel, A. Hoffmann, Fracture strength and microstructure of ODS tungsten alloys, Int. J. Refract. Met. Hard Mater. 28 (2010) 687–691, http://dx.doi.org/10.1016/j.ijrmhm.2010.05.009.

[15] Y. Lu, S. Guan, L. Hao, H. Yoshida, Review on the Photocatalyst coatings of TiO2: fabrication by mechanical coating technique and its application, CoatingsTech 5 (2015) 425–464, http://dx.doi.org/10.3390/coatings5030425.

[16] H. Yoshida, Y. Lu, H. Nakayama, M. Hirohashi, Fabrication of TiO2 film by mechanical coating technique and its photocatalytic activity, J. Alloys Compd. 475 (2009) 383–386, http://dx.doi.org/10.1016/j.jallcom.2008.07.059.

[17] D. Jeyasimman, S. Sivasankaran, K. Sivaprasad, R. Narayanasamy, R.S. Kambali, An investigation of the synthesis, consolidation and mechanical behaviour of Al 6061 nanocomposites reinforced by TiC via mechanical alloying, Mater. Des. 57 (2014) 394–404, http://dx.doi.org/10.1016/j.matdes.2013.12.067.